Antibacterial Oligomeric Polyphenols from the Green Alga *Cladophora socialis*

Serge Lavoie,[†,§,#] Anne Marie Sweeney-Jones,[‡,§] Nazia Mojib,[†,§] Brandon Dale,[∇] Kerstin Gagaring,[⊗] Case W. McNamara,[⊗] Cassandra L. Quave,[∇] Katy Soapi,[⊥] and Julia Kubanek*,[†,‡,§,∥]

[†]School of Biological Sciences and [‡]School of Chemistry and Biochemistry, Georgia Institute of Technology, Atlanta, Georgia 30332, United States

[§]Aquatic Chemical Ecology Center, Georgia Institute of Technology, Atlanta, Georgia 30332, United States

[∥]Parker H. Petit Institute for Bioengineering and Bioscience, Georgia Institute of Technology, Atlanta, Georgia 30332, United States

[⊥]Institute of Applied Sciences, University of South Pacific, Suva, Fiji

[∇]Department of Dermatology, Center for the Study of Human Health, and Antibiotic Resistance Center, Emory University, Atlanta, Georgia 30322, United States

[#]Institut des Sciences de la Forêt tempérée, Université du Québec en Outaouais, 58, rue Principale, Ripon, Québec J0V 1V0, Canada

[⊗]Calibr at The Scripps Research Institute, La Jolla, California 92037, United States

S *Supporting Information*

ABSTRACT: A series of oligomeric phenols including the known natural product 3,4,3′,4′-tetrahydroxy-1,1′-biphenyl (**3**), the previously synthesized 2,3,8,9-tetrahydroxybenzo[c]-chromen-6-one (**4**), and eight new related natural products, cladophorols B−I (**5−12**), were isolated from the Fijian green alga *Cladophora socialis* and identified by a combination of NMR spectroscopy, mass spectrometric analysis, and computational modeling using DFT calculations. *J*-resolved spectroscopy and line width reduction by picric acid addition aided in resolving the heavily overlapped aromatic signals. A panel of Gram-positive and Gram-negative pathogens used to evaluate pharmacological potential led to the determination that cladophorol C (**6**) exhibits potent antibiotic activity selective toward methicillin-resistant *Staphylococcus aureus* (MRSA) with an MIC of 1.4 μg/mL. Cladophorols B (**5**) and D−H (**7−11**) had more modest but also selective antibiotic potency. Activities of cladophorols A−I (**4−12**) were also assessed against the asexual blood stages of *Plasmodium falciparum* and revealed cladophorols A (**4**) and B (**5**) to have modest activity with EC$_{50}$ values of 0.7 and 1.9 μg/mL, respectively.
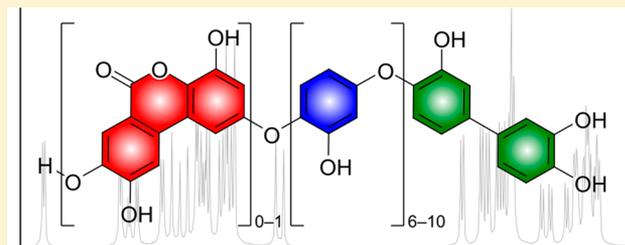
INTRODUCTION

Aromatic systems are ubiquitous within natural products, reflecting the availability of their biosynthetic precursors in plants, algae, and microorganisms via the shikimate and polyketide pathways and the varied biological effects of such functional groups.[1,2] When incorporated as building blocks in vascular plants, aromatic polymers[3−6] such as lignin provide structural support that ultimately enabled plants to occupy terrestrial ecosystems leading to the evolution of trees.[7] Aromatic natural products conferring structural rigidity were unknown in the marine realm until lignin was reported in the coralline red alga *Calliarthron cheilosporioides* (phylum Rhodophyta).[8] This startling discovery suggested that an ancestor of green and red algae acquired the capacity to polymerize phenolic monomers but that this feature was silenced in most evolving lineages. Other red algae produce a variety of structurally simple, often halogenated phenolics of mostly unknown biological function,[9] although more complex, aromatic natural products of mixed shikimate and isoprenoid biosynthetic origin have also been observed.[10] Many members of the brown algae (phylum Ochrophyta), which evolutionarily diverged just before land plants, produce polymeric, aceto-genic, phenolic compounds (phlorotannins) constituting 1−20% of dry mass.[11] These oligomers of phloroglucinol protect tissues against UV radiation and herbivory[11,12] and may contribute to structural support.[12] In contrast, significantly fewer phenolic natural products have been reported in green algae (phylum Chlorophyta). Brominated polyphenolic compounds including the feeding deterrent avrainvilleol and the condensation product of two molecules of avrainvilleol, rawsonol, are produced by green algae belonging to the genus *Avrainvillea*.[13−15] Another example of phenolic compounds from green algae are two vanillic acid analogues (**1−2**) from an Australian *Cladophora socialis* that have been found to disrupt insulin cell signaling.[16]

The present study describes a series of related oligomeric phenols, cladophorols A–I (4–12), from the green alga *C. socialis* that attracted our attention for its antibiotic activity against methicillin-resistant *Staphylococcus aureus* (MRSA). Analysis of mass spectrometric and NMR spectroscopic data enabled structure elucidation despite the high molecular weights and repeating structural patterns of members of this natural product family. We used *J*-resolved NMR spectroscopy to reduce signal overlap in the ^1H and ^{13}C NMR spectra and employed picric acid line width-narrowing to reveal the exact linkage pattern of the subunits.[17] In addition, we propose a structural revision of known vanillic acid analogues (1–2) based on a combination of spectroscopic and computational approaches.

1 R = H
2 R = SO$_3$H
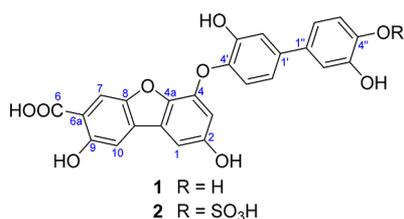
RESULTS AND DISCUSSION

Collection and Isolation. Offshore of Vanua Levu Island in Fiji, *C. socialis*, identified by morphological features and nuclear small-subunit 18S rRNA analyses (Figure S1), was collected floating at the ocean surface. The aqueous methanol extract was partitioned using a sequence of biphasic organic solvents and water. Following evaluation of MRSA activity, the ethyl acetate-soluble fraction was chromatographed on silica gel followed by repeated reversed-phase semipreparative HPLC, yielding the known compound 3,4,3′,4′-tetrahydroxy-1,1′-biphenyl (3), previously synthesized 2,3,8,9-tetrahydroxybenzo[*c*]chromen-6-one (4),[18] and eight new phenolic natural products (5–12) (Figure 1).

Characterization of 4. HRESIMS was used to assign the molecular formula of **4** as $C_{13}H_8O_6$. The ^1H NMR spectrum exhibited only four singlets at δ_H 7.58, 7.33, 7.32, and 6.73 (Table 1), attributed to two aromatic rings based on HSQC correlations with δ_C 115.4, 108.3, 107.4, and 104.4, respectively, and the absence of coupling between the protons.

Table 1. ^1H (800 MHz) and ^{13}C (200 MHz) NMR Spectroscopic Data of Cladophorols A and B (4−5) in CD$_3$OD

position	4		5	
	δ_C	δ_H	δ_C	δ_H
Benzo[*c*]chromenone				
1	107.4 (d)	7.32 s	108.2 (d)	8.37 d (2.8)
2	144.4 (s)		155.6 (s)	
3	148.6 (s)		106.9 (d)	6.69 d (2.8)
4	104.4 (d)	6.73 s	146.6 (s)	
4a	146.0 (s)		136.3 (s)	
6	164.0 (s)		163.4 (s)	
6a	112.9 (s)		114.5 (s)	
7	115.4 (d)	7.58 s	123.9 (d)	7.84 d (8.5)
8	147.3 (s)		116.4 (d)	7.08 d (8.5)
9	154.8 (s)		152.7 (s)	
10	108.3 (d)	7.33 s	144.3 (s)	
10a	131.7 (s)		123.1 (s)	
10b	111.4 (s)		120.7 (s)	
Biphenyl				
1^A			139.6 (s)	
2^A			116.0 (d)	7.14 d (2.2)
3^A			150.1 (s)	
4^A			144.0 (s)	
5^A			122.1 (d)	6.98 d (8.3)
6^A			119.1 (d)	7.02 dd (8.3, 2.2)
1^B			133.9 (s)	
2^B			114.9 (d)	7.04 d (2.2)
3^B			146.5 (s)	
4^B			145.9 (s)	
5^B			116.6 (d)	6.82 d (8.2)
6^B			119.2 (d)	6.93 dd (8.2, 2.2)

Correlations observed in HMBC from the signal at δ_H 6.73 (H-4) to δ_C 111.4 (C-10b), 144.4 (C-2), 146.0 (C-4a), and 148.6 (C-3) established the first ring. The second ring was determined from HMBC correlations from δ_H 7.58 (H-7) to δ_C 131.7 (C-10a), 147.3 (C-8), 154.8 (C-9), and 164.0 (C-6). Direct linkage between the two aromatic rings was established by HMBC correlations from δ_H 7.32 (H-1) to C-10a and from δ_H 7.33 (H-10) to C-10b. With connectivity of the carbonyl functionality and the two aromatic rings established, a third
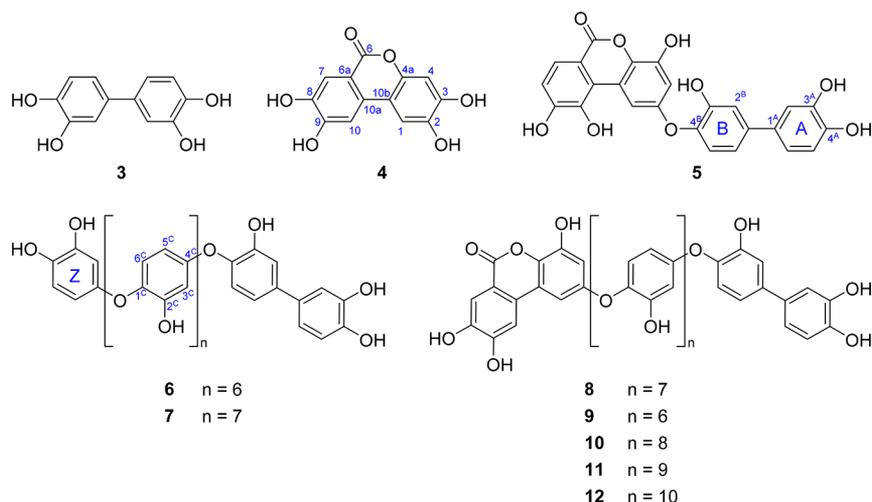

Figure 1. Structures of compounds 3−12 from *C. socialis*.

ring was necessary to account for the 10 degrees of unsaturation calculated for this compound.

Since the ^{1}H and ^{13}C NMR chemical shifts of **4** were similar to those reported for **1**, the structure depicted in Figure 2a was
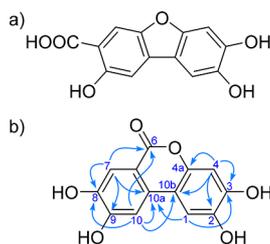

Figure 2. Possible structures (a and b) for cladophorol A (**4**) based on selected observed HMBC correlations indicated by arrows.

considered. Although it did not conflict with any of the observed NMR spectroscopic features, full consideration of all plausible structures and evaluation of these data to determine the best fit led to a more plausible alternative (Figure 2b). An HMBC spectrum recorded in DMSO-d_6 with picric acid,[17] which reduced the line widths of the phenolic hydroxy region, revealed four exchangeable protons at δ_H 10.41, 9.89, 9.74, and 9.23, each correlating with three carbons (Figure S13). In the originally considered structure (Figure 2a), only three hydroxyl groups are within this range; the carboxylic acid group is expected to shift the fourth labile proton downfield. Additionally, HMBC signals from δ_H 9.89 to C-7, C-8, and C-9 indicated an alcohol group at C-8. Since none of the labile protons correlated with carbonyl C-6, we concluded that it was part of the third ring. Compound **4** was thus identified as 2,3,8,9-tetrahydroxybenzo[c]chromen-6-one and named cladophorol A. This compound was previously reported as a synthetic analogue of ellagic acid created to improve potency for DNA gyrase inhibition, but the spectroscopic data were not disclosed at that time.[18]

Characterization of 5. Compound **5** was obtained as a pale red amorphous solid with a molecular formula of $C_{25}H_{16}O_9$ deduced by HRESIMS. The ^{1}H and COSY NMR spectra exhibited resonances accounting for four aromatic rings. [1]H–[1]H coupling constants were used to establish substitution patterns including one 1,2,3,5-tetrasubstituted ring, one 1,2,3,4-tetrasubstituted ring, and two 1,2,4-trisubstituted rings. HMBC correlations from H-1 to δ_C 123.1 (C-10a), 136.3 (C-4a), and 155.6 (C-2), from H-7 to C-10a, δ_C 152.7 (C-9), and 163.4 (C-6), and from H-8 to 114.5 (C-6a) and 144.3 (C-10) indicated the first two rings were connected in a benzo[c]chromen-6-one moiety similar to **4** (Figure S2), although the location of hydroxy groups differed with substitution at positions C-2, C-4, C-9, and C-10. The two other rings formed a biphenyl group based on HMBC correlations from H-2[A] and H-6[A] to δ_C 133.9 (C-1[B]), from H-5[A] to δ_C 139.6 (C-1[A]), from H-2[B] and H-6[B] to C-1[A], and from H-5[B] to C-1[B]. Despite careful examination of the HMBC spectra, a connecting point between the biphenyl and benzo[c]chromen-6-one could not be identified. Whereas a [4]J correlation was reported between H-5′ and C-4 for **1**,[16] a similar correlation was not found in **5**, despite recording HMBC spectra in DMSO-d_6 or acetone-d_6 and optimizing for 2 Hz long-range coupling. Adding picric acid to DMSO-d_6 for the NMR acquisition led to six labile proton signals (Figure S23) which showed correlations with all carbons bearing an

alcohol group and their neighbor (Figure S25). The four singlets at δ_H 11.04, 9.99, 9.68, and 9.57 exhibited HMBC correlations with δ_C 106.9 (C-3), 146.6 (C-4), C-4a, 116.4 (C-8), C-9, C-10, C-10a, 116.0 (C-2[B]), 150.1 (C-3[B]), and 144.0 (C-4[B]), clarifying that the benzo[c]chromen-6-one and the biphenyl were linked via an oxygen attached to C-2 and C-4[B]. For this reason, **5** was identified as 4,9,10-trihydroxy-2-[(3,3′,4′-trihydroxy-(1,1′-biphenyl)-4-yl)oxy]benzo[c]-chromen-6-one and named cladophorol B.

Structure Revision of 1. Since **4** and **5** were well characterized, the validity of the structure previously reported for **1** was questioned.[16] When recorded in DMSO-d_6, the carboxyl carbons of **4** and **5**, which are part of a lactone ring, produced NMR signals at δ_C 164.5 and 160.3, respectively. The carboxyl carbon of **1** was reported at δ_C 161.1, a value upfield of expectations for a free carboxylic acid.[16] DFT calculations of the ^{1}H and ^{13}C chemical shift values were performed for the published structure **1** and for two other hypothetical structures (**13** and **14**) having a benzo[c]-chromen-6-one unit (Figure 3,).[19,20] Indeed, the
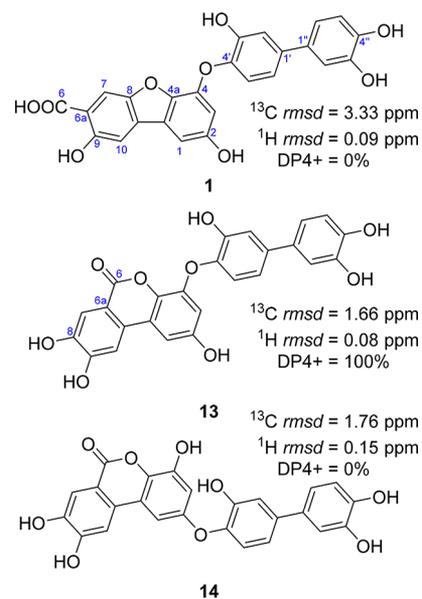

Figure 3. Original and hypothetical structures proposed for **1**, supporting reassignment of previously published **1** as **13**.

mPW1PW91/6-311+G(d,p) ^{13}C chemical shift values did not match the experimental values for the originally published structure **1** with an rmsd of 3.3 ppm (Table 2). The largest discrepancies were due to C-4a and C-6 which are involved in the lactone ring. The hypothetical structures **13** and **14** showed smaller deviations for δ_C with rmsd of 1.7 and 1.8 ppm, respectively, but only **13** exhibited a small δ_H rmsd (0.08 ppm). When DP4+ probabilities were calculated, structure **13** scored 100% when considering chemical shift data for both ^{1}H and [13]C. For this reason, **1** should be revised to **13** and named 2,8,9-trihydroxy-4-((3,3′,4′-trihydroxy[1,1′-biphenyl]-4-yl)-oxy)benzo[c]chromen-6-one.

Characterization of 6. Compound **6** was isolated as a pale red solid with a molecular formula of $C_{54}H_{38}O_{18}$ based on an $[M - H]^-$ pseudomolecular ion in the HRESIMS at m/z 973.1967. The ^{1}H NMR spectrum was difficult to interpret because of severe signal overlap in the aromatic region. J-resolved 2D NMR spectroscopy aided the interpretation and

Table 2. Experimental and Calculated NMR Chemical Shifts for 1, 13, and 14

position	exp.[16]	1		13		14	
		calc.	Δ	calc.	Δ	calc.	Δ
$\delta_H{}^a$							
H-1	6.92	7.00	−0.08	7.01	−0.09	6.71	+0.21
H-3	6.55	6.61	−0.06	6.47	+0.08	6.83	−0.28
H-7	7.55	7.63	−0.08	7.47	+0.08	7.59	−0.04
H-10	7.38	7.22	+0.16	7.35	+0.03	7.10	+0.28
H-2^A	6.96	6.92	+0.04	6.92	+0.04	7.02	−0.06
H-5^A	6.80	6.88	−0.08	6.89	−0.09	6.84	−0.04
H-6^A	6.87	6.99	−0.12	7.04	−0.17	7.01	−0.14
H-2^B	7.14	7.11	+0.03	7.15	−0.01	7.12	+0.02
H-5^B	7.00	6.94	+0.06	6.97	+0.03	6.99	+0.01
H-6^B	7.04	6.89	+0.15	6.96	+0.08	6.99	+0.05
	rmsd[b]	0.09		0.08		0.15	
	MAE[c]	0.16		0.17		0.28	
	DP4+ [1]H data[d]	3.7 %		96.3 %		0.0 %	
δ_C							
C-1	98.7	102.1	−3.4	100.2	−1.5	97.7	+1.0
C-2	154.2	150.3	+3.9	153.5	+0.7	155.6	−1.4
C-3	104.2	106.4	−2.2	103.6	+0.6	104.8	−0.6
C-4	145.9	140.5	+5.4	146.3	−0.4	145.5	+0.4
C-4a	134.0	140.1	−6.1	135.9	−1.9	134.3	−0.3
C-6	161.1	166.7	−5.6	160.7	+0.4	159.5	+1.6
C-6a	112.8	108.3	+4.5	112.2	+0.6	113.0	−0.2
C-7	114.0	113.2	+0.8	113.3	+0.7	114.6	−0.6
C-8	146.9	145.4	+1.5	144.2	+2.7	144.4	+2.5
C-9	152.6	155.8	−3.2	151.6	+1.0	150.8	+1.8
C-10	107.9	108.3	−0.4	107.1	+0.8	107.0	+0.9
C-10a	128.1	130.7	−2.6	129.5	−1.4	129.6	−1.5
C-10b	118.6	124.4	−5.8	119.8	−1.2	118.4	+0.2
C-1^A	130.6	131.5	−0.9	133.8	−3.2	133.7	−3.1
C-2^A	113.7	112.4	+1.3	112.3	+1.4	112.1	+1.6
C-3^A	145.5	140.5	+5.0	143.8	+1.7	143.7	+1.8
C-4^A	144.6	141.7	+2.9	144.0	+0.6	143.6	+1.0
C-5^A	115.5	114.4	+1.1	113.6	+1.9	114.0	+1.5
C-6^A	116.9	119.7	−2.8	119.7	−2.8	119.2	−2.3
C-1^B	137.8	137.9	−0.1	139.9	−2.1	140.6	−2.8
C-2^B	114.6	114.1	+0.5	113.4	+1.2	113.8	+0.8
C-3^B	148.7	145.7	+3.0	149.4	−0.7	150.1	−1.4
C-4^B	141.1	138.9	+2.2	141.2	−0.1	140.6	+0.5
C-5^B	116.8	118.9	−2.1	119.1	−2.3	120.9	−4.1
C-6^B	121.3	118.1	+3.2	118.1	+3.2	118.6	+2.7
	rmsd[b]	3.3		1.7		1.8	
	MAE[c]	6.1		3.2		4.1	
	DP4+ [13]C data[d]	0.0 %		96.8 %		3.2 %	
	DP4+ all data[d]	0.0 %		100.0 %		0.0 %	

[a]δ values calculated at the mPW1PW91/6-311+G(d,p)//B3LYP/6-31G(d) level of theory performed with the polarizable continuum model (PCM) using DMSO. Red color highlights large differences in calculated values: $|\Delta\delta_H| > 0.2$, $|\Delta\delta_C| > 3.0$. [b]Root-mean-square deviation. [c]Maximum absolute error. [d]DP4+ probability.[21]

allowed assignment of all chemical shifts and coupling constants (Table 3). Using DQF-COSY and J-resolved spectroscopy, seven AMX aromatic spin systems resulting from 1,2,4-trihydroxyphenyl groups were observed as doublets at δ_H 6.67−6.91 and 6.42−6.57 and doublet of doublets at δ_H 6.27−6.47. Interestingly, within each of these ranges, a gradient of proton chemical shifts was noted whereby each set of signals from a given ring appeared in a predictable order. This feature was highlighted by simulating each set of protons using the extracted δ_C and J from NMR spectra (Figure 4). When comparing proton signals for H-3, H-5, and H-6, the two signals corresponding to rings Y and Z appeared to be outliers.

Most of the carbon signals were resolved in the ^{13}C NMR spectrum, although HSQC and HMBC spectra showed large clusters of correlations between protons of rings D−G and carbons averaged at 157.5 (C-4$^{D−G}$), δ_C 151.2 (C-2$^{D−G}$), 139.6 (C-1$^{D−G}$), 123.1 (C-6$^{D−G}$), 108.8 (C-5$^{D−G}$), and 106.4 (C-3$^{D−G}$). This prevented a precise assignment of signals but also indicated these rings were similar. Two other spin systems unrelated to the gradient of chemical shifts showed HMBC correlations from H-2^A to δ_C 139.9 (C-1^B) and from H-2^B and H-6^B to δ_C 133.9 (C-1^A) allowing assignment of these two spin systems to a biphenyl unit (Figure S2). Given all these data,

Table 3. ^{1}H (800 MHz) and ^{13}C (200 MHz) NMR Spectroscopic Data of Cladophorols C and D (6−7) in CD$_3$OD

position	6 δ_C	6 δ_H	7 δ_C	7 δ_H
Rings A−B (Biphenyl)				
1^A	134.0		134.0	
2^A	114.9	7.01 (d, 2.2)	114.9	7.01 (d, 2.2)
3^A	146.5		146.5	
4^A	146.0		146.0	
5^A	116.6	6.81 (d, 8.2)	116.6	6.81 (d, 8.2)
6^A	119.3	6.91$_2$ (dd, 8.2, 2.2)	119.3	6.91$_2$ (dd, 8.2, 2.3)
1^B	139.9		139.9	
2^B	116.1	7.11 (d, 2.2)	116.1	7.11 (d, 2.2)
3^B	150.2		150.2	
4^B	143.9		143.9	
5^B	122.3	6.94 (d, 8.3)	122.2	6.94 (d, 8.3)
6^B	119.2	7.00 (dd, 8.3, 2.2)	119.2	7.00 (dd, 8.3, 2.2)
Ring C				
1	139.8		139.8$_7$	
2	151.3		151.3	
3	107.0	6.57 (d, 2.9)	107.0	6.58 (d, 2.9)
4	157.0		157.0	
5	109.4	6.47 (dd, 8.8, 2.9)	109.4	6.47 (dd, 8.8, 2.9)
6	123.2^b	6.90$_5$ (dd, 8.8)	123.2^b	6.90$_5$ (dd, 8.8)
Middle Rings				
1	139.7, 139.5$_4$, 139.5$_3$, 139.5$_0$		139.7$_6$, 139.5$_7$, 139.5$_5$, 139.5$_2$ (2×)	
2	151.2$_5$, 151.2$_3$, 151.2$_1$, 151.1		151.2$_6$, 151.2$_4$, 151.2$_3$, 151.2$_1$, 151.1	
3	106.5, 106.3$_6$, 106.3$_4$, 106.3$_1$	6.53, 6.51, 6.50$_3$, 6.49$_6$ (all d, 2.9)	106.5 (2×), 106.3$_7$, 106.3$_6$, 106.3$_3$	6.53, 6.51$_2$, 6.51, 6.50$_3$, 6.49$_7$ (all d, 2.9)
4	157.6, 157.5$_4$, 157.5$_1$, 157.4,		157.6 (2×), 157.5$_4$, 157.5$_1$, 157.4	
5	108.8, 108.7$_7$, 108.7$_5$, 108.7$_4$	6.42, 6.41, 6.40, 6.39 (all dd, 8.8, 2.9)	108.8, 108.7$_8$, 108.7$_7$ (2×), 108.7$_5$	6.42$_3$, 6.41, 6.40, 6.39$_9$, 6.38$_8$ (all dd, 8.8, 2.9),
6	123.1$_9$ (2×), 123.1$_4$, 122.9	6.88, 6.87, 6.86, 6.84 (all d, 8.8)	123.1$_9$ (2×), 123.1$_7$, 123.1$_3$, 122.9	6.88, 6.87, 6.86$_8$, 6.86$_3$, 6.84 (all d, 8.8)
Ring Y^a				
1	141.0		141.0	
2	150.6		150.6	
3	106.3$_4$^{b}	6.48 (d, 2.9)	106.3$_6$^{b}	6.48 (d, 2.9)
4	156.7		156.7	
5	108.6$_6$^{b}	6.34 (dd, 8.8, 2.9)	108.6$_8$^{b}	6.34 (dd, 8.8, 2.9)
6	121.7	6.74 (d, 8.8)	121.7	6.74 (d, 8.8)
Ring Z^a				
1	141.7		141.7	
2	147.0		147.0	
3	106.4^b	6.42 (d, 2.9)	106.4$_5$^{b}	6.42$_0$ (d, 2.9)
4	152.9		152.9	
5	109.1	6.27 (dd, 8.6, 2.9)	109.1	6.27 (d, 8.6, 2.9)
6	116.4	6.67 (d, 8.6)	116.4	6.67 (d, 8.6)

^{a}Rings Y and Z are the last two rings of the oligomer. ^{b}^{13}C signal can be interchanged with one of the corresponding signals of rings D−G.

two structures were hypothesized, differing by the position of the free alcohol groups on each hydroxyphenyl (Figure 5).

Two model structures, **15a** and **15b**, containing a biphenyl unit and three 1,2,4-trihydroxyphenyl rings (Figure 5), were computationally tested to determine which arrangement was more probable. Their ^{1}H and ^{13}C NMR chemical shifts were predicted (Tables S26 and S27) following DFT computation at the mPW1PW91/6-311+G(d,p) level of theory and compared to the corresponding position of **6**. The rmsd and MAE values calculated for both ^{1}H and ^{13}C were lower when **15a** was considered, indicating that **6a** is the correct structure. Based on these results, **6** was identified as α-hydro-ω-[3,4-dihydroxyphenyl]octa[oxy(2-hydroxyphen-4-yl)] and named cladophorol C.

Characterization of 7. The molecular formula for **7** was established as $C_{60}H_{42}O_{20}$ based on HRESIMS, accounting for one additional dihydroxyphenyl moiety. The ^{1}H and ^{13}C NMR spectra almost perfectly superimposed those of **6**, the only differences being three additional proton signals at δ_H 6.86 (d, $J = 8.8$ Hz), 6.50 (d, $J = 2.9$ Hz), and 6.40 (dd, $J = 8.8$ Hz) and six additional carbon signals at δ_C 157.6, 151.2$_3$, 139.5$_7$, 123.1$_7$, 108.7$_7$, and 106.5. As a result, **7** was identified as α-hydro-ω-[3,4-dihydroxyphenyl]nona[oxy(2-hydroxyphen-4-yl)] and named cladophorol D.

Characterization of 8. Compound **8** was isolated as a reddish solid with the molecular formula $C_{67}H_{44}O_{23}$ based on an [M − H]$^-$ HRESIMS peak at m/z 1215.2188. The ^{1}H and ^{13}C NMR spectra strongly resembled those of **6** and **7**,
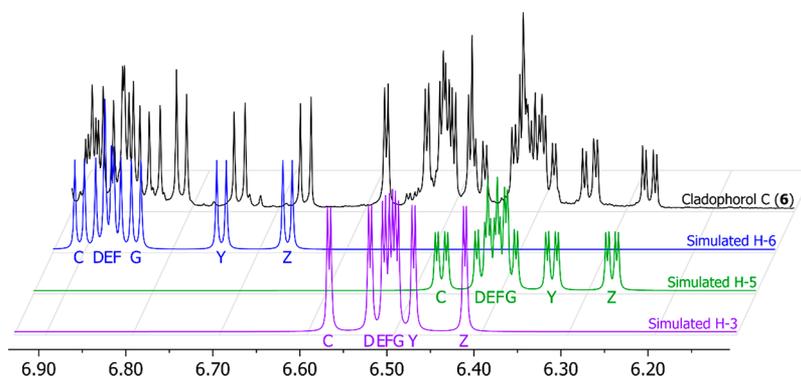
Figure 4. Gradient of NMR chemical shift along the oligomer of 1,2,4-trihydroxyphenyl units for cladophorol C (**6**). Experimental (black) and simulated (colored) signals are shown.
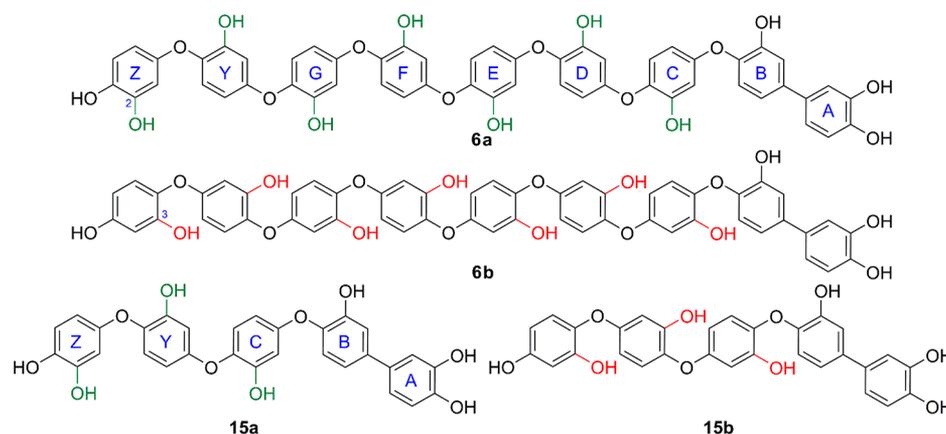

Figure 5. Hypothetical structures for cladophorol C (**6a** and **6b**) and model structures **15a** and **15b**.

suggesting that **8** was also an oligomeric phenolic with a terminal biphenyl. A limited spread of the signals for the repeating phenol units, as illustrated by the ¹H spectral comparison of H-6 (Figure 6), suggested an end-capping of the
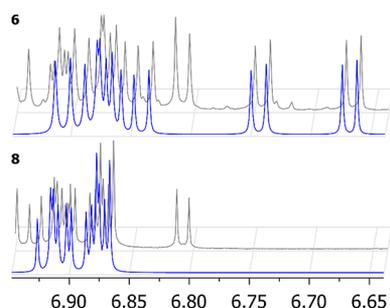
Figure 6. Chemical shift spreading for cladophorol C (**6**) and cladophorol E (**8**) for position H-6. The limited spreading of **8** suggest an end-capping of the oligomer. Simulated (blue) and experimental (gray) signals are shown.

oligomer with a different moiety. A carbonyl, indicated by a peak on the ¹³C NMR spectrum at δ_C 163.4, and 12 other distinct ¹³C NMR signals, agreed with a benzo[c]chromen-6-one unit (Table 4). The substitution pattern was determined as 2,4,8,9-tetrahydroxy- from the presence of two distinct singlets at δ_H 7.63 and 7.32 and two doublets at δ_H 6.96 and 6.55 (both J = 2.7 Hz) in the ¹H NMR spectrum (Table 5). This assignment was corroborated by HMBC correlations from H-1 and H-3 to δ_C 136.2 (C-4a) and from H-1 to δ_C 130.7 (C-10a)

(Figure S2). This benzo[c]chromen-6-one group matched revised structures **13** and **14**; however, the exact point of attachment of the oligomer needed to be established to determine which configuration was more probable for **8**. A comparison of ¹³C NMR values of **8** recorded in DMSO-d_6 and those reported for **13**[16] (Table S1) showed the greatest differences at C-2, C-4, and C-6, suggesting the oligomer was attached to C-2 as in **14** instead of C-4. When the calculated values for **13** and **14** were considered, a 94% DP+ value favoring **14** confirmed this hypothesis. For this reason, **8** was identified as α-[(4,8,9-trihydroxy-2-benzo[c]chromen-6-on-2-yl)oxy]-ω-[3,4-dihydroxyphenyl]octa[oxy(2-hydroxyphen-4-yl)] and named cladophorol E.

Characterization of 9−12. Compounds **9−12** each exhibited ¹H and ¹³C NMR spectra similar to that of **8** (Tables 4 and 5). Proton integrations in the three overlapping regions (δ_H 6.85−6.98, 6.49−6.56, and 6.39−6.45) indicated three fewer protons for **9** and 3, 6, and 9 additional protons for **10−12**. This suggested **9−12** were members of a series with **8**, which was further supported by high-resolution mass spectrometry with [M − H]⁻ ions at m/z 1107.1973, 1323.2394, 1431.2617, and 1539.2797 for **9−12**, respectively. Since **10** was more abundant than the other members of the series, its NMR spectra in DMSO-d_6 doped with picric acid were recorded (Figure S70). Three labile protons at δ_H 10.52, 10.16, and 10.11 correlated with δ_C 153.1 (C-9), 147.4 (C-8), 146.1 (C-4), 134.4 (C-4a), 114.5 (C-7), 107.9 (C-10), and 103.7 (C-3), indicating a substituted oxygen attached to C-2 as determined previously from the comparison of chemical shifts of **8** with experimental and calculated values of **13** and **14**

Table 4. ^{13}C (200 MHz) NMR Spectroscopic Data of Cladophorols E–I (8–12) in CD$_3$OD

position	8	9	10	11	12
Rings A–B (Biphenyl)					
1^A	134.0	134.0	134.0	134.0	134.0
2^A	114.9	114.9	114.9	114.9	114.9
3^A	146.5	146.5	146.5	146.5	146.5
4^A	146.0	146.0	146.0	146.0	146.0
5^A	116.6	116.7	116.6	116.6	116.6
6^A	119.3	119.3	119.3	119.3	119.3
1^B	139.9$_3$	139.9$_1$	139.9$_2$	139.9$_2$	139.9$_3$
2^B	116.1	116.1	116.1	116.1	116.1
3^B	150.2$_1$	150.2	150.2$_0$	150.2	150.2$_3$
4^B	143.9	143.9	143.9	143.9	143.9
5^B	122.2	122.2	122.2	122.2	122.3
6^B	119.2	119.2	119.2	119.2	119.2
Middle Rings					
1	139.8$_7$, 139.6, 139.5$_2$, 139.5$_0$, 139.4$_9$, 139.3$_8$, 139.2	139.8$_7$, 139.6, 139.5, 139.4$_8$, 139.3$_8$, 139.2	139.8$_6$, 139.6, 139.5, 139.4$_9$ (2×), 139.4$_8$, 139.3$_7$, 139.2	139.8$_6$, 139.6, 139.4$_9$ (4×), 139.4$_7$, 139.3$_6$, 139.2	139.85, 139.5, 139.48 (5×), 139.46, 139.36, 139.2
2	151.3$_2$, 151.3$_0$, 151.2$_7$, 151.2$_5$, 151.2$_3$ (3×)	151.3, 151.2$_8$, 151.2$_6$, 151.2$_3$, 151.2$_2$ (2×)	151.3, 151.2$_9$, 151.2$_7$, 151.2$_4$, 151.22 (4×)	151.3$_2$, 151.3$_0$, 151.2$_7$, 151.2$_4$, 151.23 (3×), 151.2$_2$ (2×)	151.33, 151.31, 151.28, 151.25, 151.24 (6×)
3	107.0, 106.5, 106.3$_8$ (3×), 106.3$_7$ (2×)	107.1, 106.5, 106.3$_9$, 106.3$_8$, 106.3$_7$ (2×)	107.0, 106.4, 106.3$_7$ (3×), 106.3$_6$ (3×)	107.0, 106.4, 106.3$_7$ (2×), 106.3$_6$ (5×)	107.0, 106.4, 106.3 (8×)
4	157.8, 157.7, 157.5$_9$, 157.5$_7$, 157.5$_6$, 157.5$_0$, 157.0	157.8, 157.6, 157.5$_7$, 157.5$_5$, 157.4$_9$, 157.0	157.8, 157.6$_5$, 157.5$_8$, 157.5$_7$, 157.5$_6$ (2×), 157.5$_0$, 157.0	157.8, 157.6, 157.5$_8$, 157.5$_6$ (4×), 157.5$_0$, 157.0	157.8, 157.7, 157.58 (3), 157.57 (3×), 157.52, 157.0
5	109.4, 108.8$_5$, 108.8$_1$, 108.7$_9$ (2×), 108.7$_8$ (2×)	109.4, 108.8$_4$, 108.8$_0$, 108.7$_9$, 108.7$_8$, 108.7$_7$	109.4, 108.8$_4$, 108.8$_0$, 108.7$_8$, 108.77 (4×)	109.4, 108.8$_4$, 108.8$_0$, 108.7$_8$, 108.7$_7$ (5×)	109.4, 108.8, 108.79, 108.76 (7×)
6	123.4, 123.3, 123.2$_0$ (3×), 123.1$_8$ (2×)	123.4, 123.3, 123.2$_0$ (3×), 123.1$_9$	123.4, 123.3, 123.2$_0$ (3×), 123.1$_9$ (3×)	123.4, 123.3, 123.2$_0$, 123.1$_8$ (6×)	123.41, 123.35, 123.22 (2), 123.20 (6×)
Benzo[c]chromenone					
1	100.4	100.4	100.4	100.4	100.4
2	156.9	156.9	156.9	156.9	156.9
3	105.8	105.8	105.8	105.8	105.8
4	147.5	147.5	147.5	147.5	136.2
4a	136.2	136.2	136.2	136.2	147.5
6	162.7	162.8	162.8	162.7	162.7
6a	114.5	114.4	114.5	114.5	114.5
7	115.6	115.5	115.6	115.6	115.6
8	148.6	148.7	148.6	148.6	148.7
9	154.6	155.3	154.6	154.6	154.6
10	108.6	108.6	108.6	108.6	108.6
10a	130.7	130.7	130.7	130.7	130.7
10b	120.7	120.7	120.7	120.7	120.7

(Figure S2). Altogether, these data supported the assignment of these natural products as α-[(4,8,9-trihydroxy-2-benzo[c]-chromen-6-on-2-yl)oxy]-ω-[3,4-dihydroxyphenyl]hepta[oxy-(2-hydroxyphen-4-yl)] (**9**), α-[(4,8,9-trihydroxy-2-benzo[c]-chromen-6-on-2-yl)oxy]-ω-[3,4-dihydroxyphenyl]nona[oxy(2-hydroxyphen-4-yl)] (**10**), α-[(4,8,9-trihydroxy-2-benzo[c]-chromen-6-on-2-yl)oxy]-ω-[3,4-dihydroxyphenyl]deca[oxy(2-hydroxyphen-4-yl)] (**11**), and α-[(4,8,9-trihydroxy-2-benzo-[c]chromen-6-on-2-yl)oxy]-ω-[3,4-dihydroxyphenyl]undeca-[oxy(2-hydroxyphen-4-yl)] (**12**) and named cladophorols F–I.

Pharmacological Assays. The antimicrobial activities of all isolated natural products (**3–12**) were assessed against multiple drug-resistant (MDR) Gram-positive and Gram-negative human pathogens as well as amphotericin-resistant *Candida albicans* (Table 6, Figure S3). Cladophorol C (**6**) was found to be very potent only against MRSA with a minimal inhibitory concentration (MIC) value of 1.4 μg/mL. The bioactivity is negatively correlated by the presence of a benzo[c]chromen-6-one unit, as shown by the weaker MIC values for **5** and **8–12** (13–49 μg/mL) relative to **6** and **7**

(1.4–9 μg/mL)). The total number of phenol rings is also an important factor since the most potent compounds in both series (**6–7** vs **8–12**) have 9–10 rings and the activity weakens as this number increases. Surprisingly, all of the other cell lines, including the other Gram-positive bacterium, VREF, were much less sensitive to this family of natural products. The bioactivities of **4–12** were also evaluated in an assay using intraerythrocytic *Plasmodium falciparum*.[22] Only **4** and **5** inhibited the parasite with half-maximal effective concentration (EC$_{50}$) values of 0.7 and 1.9 μg/mL, respectively. In addition, the cytotoxicities of **3–12** were evaluated using immortalized human keratinocytes (HaCaT) and human kidney cells (HEK293T). Although compounds **5–11** exhibited weak toxicity (<25%) at their respective maximum concentrations against HaCaT (Figure 7) and **4** and **5** had weak toxicity toward HEK293T (half maximal cytotoxicity concentration (CC$_{50}$) of 9.4 and 4.5 μg/mL, respectively), no toxicity was observed at the MRSA MICs for **5–11** or the *P. falciparum* EC$_{50}$ values for **4** and **5**.

Table 5. ^{1}H (800 MHz) NMR Spectroscopic Data of Cladophorols E−I (8−12) in CD_3OD

position	8	9	10	11	12
Rings A–B (Biphenyl)					
2^A	7.01 (d, 2.2)	7.02 (d, 2.2)	7.02 (d, 2.2)	7.01 (d, 2.2)	7.01 (d, 2.2)
5^A	6.81 (d, 8.2)	6.81 (d, 8.2)	6.81 (d, 8.2)	6.81 (d, 8.2)	6.81 (d, 8.2)
6^A	6.91 (dd, 8.2, 2.4)	6.91 (dd, 8.2, 2.2)	6.91_3 (dd, 8.2, 2.2)	6.91_0 (dd, 8.2, 2.2)	6.91 (dd, 8.2, 2.3)
2^B	7.11 (d, 2.2)	7.11 (d, 2.2)	7.11 (d, 2.2)	7.11 (d, 2.2)	7.11 (d, 2.3)
5^B	6.94 (d, 8.3)	6.94 (d, 8.3)	6.94 (d, 8.3)	6.94 (d, 8.3)	6.94 (d, 8.3)
6^B	7.00 (dd, 8.4, 2.2)	7.00 (dd, 8.3, 2.2)	7.00 (dd, 8.3, 2.2)	7.00 (dd, 8.3, 2.2)	7.00 (dd, 8.3, 2.2)
Middle Rings					
3	6.58, 6.54, 6.53, 6.52, 6.51_3, 6.51_1, 6.51_0 (all d, 2.9)	6.58, 6.54, 6.53, 6.52, 6.51_7, 6.51_4 (all d, 2.9)	6.58, 6.54_5, 6.53, 6.52_5, 6.51_6, 6.51_4, 6.51_1 (2×) (all d, 2.9)	6.57, 6.54, 6.53, 6.52, 6.51_1, 6.51_0, 6.50_6, 6.50_4 (2×) (all d, 2.9)	6.57, 6.54, 6.53, 6.52, 6.51, 6.50_8, 6.50_6 (2×), 6.50_4 (2×) (all d, 2.9)
5	6.47, 6.44, 6.42_3, 6.42_2, 6.40_9, 6.40_7, 6.40_5 (all dd, 8.8, 2.9)	6.47, 6.43, 6.42_3, 6.42_2, 6.41_0, 6.40_7 (all dd, 8.8, 2.9)	6.47, 6.44, 6.43, 6.42, 6.41, 6.40_9, 6.40_8, 6.40_6 (all dd, 8.8, 2.9)	6.47, 6.43, 6.42_3, 6.42_1, 6.40_7, 6.40_5, 6.40_3, 6.40_2 (2×) (all dd, 8.8, 2.9)	6.47, 6.43, 6.42_2, 6.42_1, 6.40_7, 6.40_5, 6.40_3, 6.40_1 (3×) (all dd, 8.8, 2.9)
6	6.92, 6.91, 6.90, 6.88, 6.87_6, 6.87_2 (2×) (all d, 8.8)	6.92, 6.90_8, 6.90_5, 6.88, 6.87_7, 6.87_5 (all d, 8.8)	6.92, 6.91_1, 6.90_7, 6.88, 6.87_9, 6.87_5 (2×), 6.87_2 (all d, 8.8)	6.92, 6.91, 6.90, 6.88, 6.87_6, 6.87_1 (2×), 6.86_8 (2×) (all d, 8.8)	6.92, 6.90_8, 6.90_5, 6.88, 6.87_6, 6.87_1 (2×), 6.86_9 (3×) (all d, 8.8)
Benzo[c]chromenone					
1	6.96 (d, 2.7)	6.96 (d, 2.7)	6.96 (d, 2.7)	6.96 (d, 2.7)	6.96 (d, 2.8)
3	6.55 (d, 2.7)	6.55 (d, 2.7)	6.55_2 (d, 2.7)	6.55_0 (d, 2.7)	6.55 (d, 2.7)
7	7.63 (s)	7.63 (s)	7.64 (s)	7.63 (s)	7.63 (s)
10	7.32 (s)	7.32 (s)	7.33 (s)	7.32 (s)	7.33 (s)

Table 6. Pharmacological Activities^a of 3,4,3′,4′-Tetrahydroxy-1,1′-biphenyl (3) and Cladophorols A−I (4−12)

		microbial strains^c					
compd	no. of rings^b	MRSA	VREF	Gram−	WTCA	ARCA	*P. falciparum*^{d}
3	2	>50	>50	>50	>50	>50	NT
4	2	>50	>50	>50	>50	>50	0.7 ± 0.1
5	4	13 ± 2	>50	>50	>50	>50	1.9 ± 0.2
6	9	1.4 ± 0.3	>50	>50	46 ± 13	46 ± 9	>2
7	10	9 ± 2	>50	>50	>50	>50	>2
8^e	11	25 ± 3	>50	>50	>50	>50	>2
9	10	14 ± 3	>50	>50	>50	>50	>2
10	12	31 ± 3	>50	>50	>50	>50	>2
11	13	49 ± 8	>50	>50	>50	>50	>2
12^e	14	>50	>50	>50^e	>50	>50	>2

^{a}The values are expressed as a 95% confidence interval. ^{b}Total number of phenyl rings. ^{c}Minimal inhibitory concentration (μg/mL). Cell lines are MRSA = methicillin-resistant *Staphylococcus aureus*; VREF = vancomycin-resistant *Enterococcus faecium*; Gram−: [*Escherichia coli*; multiple drug-resistant (MDR) *E. coli*; MDR *Klebsiella pneumonia*; MDR *K. pneumonia*; MDR *Acinetobacter baumannii*; *A. baumannii*; MDR *Enterobacter aerogenes*; MDR *Enterobacter cloacae*; wild type *Pseudomonas aeruginosa*]; WTCA = wild type *Candida albicans*; ARCA = amphotericin B-resistant *C. albicans*. Details for the positive controls are provided in the Experimental Section. ^{d}Half-maximal effective concentration (μg/mL). ^{e}Tested only against *E. coli*.

■ EXPERIMENTAL DETAILS

General Experimental Procedures. NMR spectra (^{1}H, HMBC, HSQC, DQF-COSY, and J-resolved) were recorded on an 18.8 T (800 MHz for ^{1}H and 200 MHz for ^{13}C) Bruker Avance IIIHD 800 instrument equipped with a 5 mm triple resonance broadband cryoprobe. All spectra were acquired in CD_3OD or DMSO-d_6, and chemical shifts were reported in ppm (δ) relative to the residual solvent peaks (δ_H 3.31 and δ_C 49.00 for CD_3OD, δ_H 2.50 and δ_C 39.52 for DMSO-d_6). All spectra were processed using MestReNova 11.0. HPLC separations were performed with a Waters 1525 binary pump and a Waters 2487 dual wavelength absorbance detector set at 260 nm, using two different columns: a 9.4 × 250 mm, C_{18} silica reversed-phase (Zorbax stable-bond, 5 μm particle size), and a 4.6 × 250 mm phenylhexyl phase (Phenomenex Luna, 5 μm particle size). High-resolution mass spectrometry was conducted on an Orbitrap spectrometer in negative ion mode. The masses of isolated compounds were estimated by qNMR using a capillary filled with benzene-d_6 and calibrated against caffeine.[23]

Specimen Collection. Green alga (collection G-1240) was harvested as floating clumps on Dec 3, 2015, at the ocean surface near Titi Island, Viti Levu, Fiji (16°16′26″ S, 179°26′02″ E). This collection was identified as *Cladophora socialis* Kützing by morphological and 18S rRNA phylogenetic analyses. Voucher specimens were preserved in aqueous formaldehyde and stored at the University of South Pacific. The collection was stored at −80 °C until extraction.

Species Identification. The collected green alga (G-1240) was identified by comparing its morphological traits with that of previously described *Cladophora* species[24] and by sequence analysis of nuclear, small subunit (SSU) rRNA (18S rRNA). Genomic DNA from an ethanol-preserved algal specimen was extracted using the innuPREP plant DNA kit (Analytik Jena, Germany) according to the manufacturer's protocol. The three overlapping 18S rRNA gene fragments from genomic DNA were amplified via the polymerase chain reaction (PCR) in three separate reactions using universal primer pairs, NS3/NS4, NS5/NS6, and NS7/NS8.[25] Each PCR amplification was performed in a 25 μL reaction volume consisting of
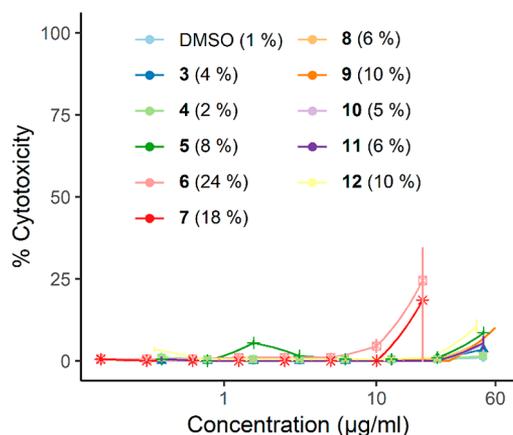
Figure 7. Cytotoxicity of **3−12** against human keratinocytes (HaCaT). The parenthetical values provide the relative cytotoxicities (%) at the maximum concentration tested (60 μg/mL for **9**, 50 μg/mL for **3−5, 8, 10, 11**, 45 μg/mL for **12**, and 20 μg/mL for **6** and **7**).

5−50 ng of purified genomic DNA; 200 μM of each of the dNTPs; 1 μM of each of the oligonucleotide primer; 1.0 U Taq DNA polymerase, and 1× standard PCR reaction buffer (NEB, Ipswich, MA). All PCR amplifications were performed in a GeneAmp PCR system 2700 (Applied Biosystems, Foster City, CA) thermocycler using the following temperature cycling parameters: initial denaturation at 94 °C for 5 min followed by a total of 40 cycles of amplification in which each cycle consisted of denaturation at 94 °C for 40 s, primer annealing at 50 °C for 40 s and primer extension at 72 °C for 1 min. After amplification, final extension of the incompletely synthesized DNA was carried out at 72 °C for 7 min. The PCR fragments were analyzed by agarose gel electrophoresis (1% wt/vol). The gel was stained with ethidium bromide and visualized under a UV transilluminator. All of the PCR fragments were either sequenced with forward or reverse primers, and sequences were manually edited and assembled using CAP3 Sequence Assembly Program.[26] The assembled G-1240 18S rRNA sequence (1334 bp) was submitted to GenBank (accession no. MK127549). The sequence similarity of the assembled contig of G-1240 18S rRNA to other known *Cladophora* spp. was determined by comparing it with the nonredundant nucleotide database (NCBI) using the blastn program.[27] The top ranked matches according to *E* values and maximum scores revealed high similarity to *C. socialis* with 96% identity.

Further, the 18S rRNA sequence of G-1240 was compared with those of other known species of the genus *Cladophora* and two outgroup taxa *Ulva curvata* and *Ulothrix zonata* from the same class but different orders, obtained from GenBank. Phylogenetic analysis was conducted in MEGA X[28] using the Maximum Likelihood method based on the Tamura−Nei model[29] with 1000 bootstrap iterations. The phylogenetic analysis revealed that G-1240 is closely related to *C. socialis* (Figure S1). Overall, morphological and phylogenetic analyses are consistent with identification of the green alga G-1240 as *C. socialis*.

Isolation of 3−12. Frozen material (659 g) was thawed and broken into small pieces (∼1 cm) before being agitated in 60% aqueous MeOH (1.3 L) for 3 days. The mixture was filtered with a metal wire mesh, and the residues were extracted four more times with pure MeOH (2 × 1 L) and CHCl3/MeOH 1:1 (2 × 1 L). The solutions were pooled, filtered, and evaporated under reduced pressure to yield a brown gummy extract (33.4 g). The residue was dissolved in MeOH/H2O 9:1 (500 mL) and partitioned with hexanes (4 × 250 mL, 1.56 g). The amount of water in the MeOH/H2O phase was increased to a 3:2 ratio, and the resulting solution was partitioned with CHCl3 (3 × 500 mL, 0.75 g). The methanol was removed from the MeOH/H2O phase by vacuum evaporation, and the aqueous phase was extracted with EtOAc (3 × 250 mL, 2.05 g). The EtOAc fraction was subjected to silica gel column chromatography eluting

with a gradient of CH2Cl2/MeOH from 49:1 to 1:2 to yield nine fractions (3.1−3.9). Fraction 3.5 (97.4 mg) was separated by reversed-phase semipreparative HPLC eluting with H2O + 0.05% TFA and MeCN (25 to 75% gradient, in 25 min). In addition to pure **3** (t_R = 3.8 min, 0.50 mg), **4** (t_R = 4.9 min, 0.68 mg), and **5** (t_R = 8.7 min, 3.4 mg), eight other fractions were collected (3.5.1−3.5.8). Fraction 3.5.1 was subjected to HPLC using a phenylhexyl column and eluting with H2O + 0.05% TFA and MeOH (75 to 85% gradient, in 15 min) to yield **6** (t_R = 7.9 min, 0.057 mg) and **11** (t_R = 12.8 min, 0.62 mg). Fraction 3.5.2 was separated by HPLC with a phenylhexyl column eluting with H2O + 0.05% TFA and MeOH (75 to 85% gradient, in 15 min) to obtain **9** (t_R = 9.5 min, 0.10 mg) and **12** (t_R = 12.8 min, 0.027 mg). The same conditions were used to purify fraction 3.5.3 yielding **7** (t_R = 9.0 min, 0.32 mg). Fraction 3.5.4 was purified by HPLC using a phenylhexyl column and eluting with H2O + 0.05% TFA and MeOH (80 to 82.5% in 7.5 min) to obtain **8** (t_R = 6.5 min, 0.60 mg). Fraction 3.5.6 was subjected to HPLC using a phenylhexyl column and eluting with H2O + 0.05% TFA and MeOH (20 to 82.5% gradient, in 7.5 min) to yield **10** (t_R = 6.4 min, 2.3 mg).

Cladophorol A (4): pale red amorphous solid; ^{1}H and ^{13}C NMR data, see Table 1; HRMS (ESI) *m/z* $[M − H]^-$ calcd for $C_{13}H_7O_6^-$ 259.0248, found 259.0245.

Cladophorol B (5): pale red amorphous solid; ^{1}H and ^{13}C NMR data, see Table 1; HRMS (ESI) *m/z* $[M − H]^-$ calcd for $C_{25}H_{15}O_9^-$ 459.0722, found 459.0718.

Cladophorol C (6): pale red amorphous solid; ^{1}H and ^{13}C NMR data, see Table 3; HRMS (ESI) *m/z* $[M − H]^-$ calcd for $C_{54}H_{37}O_{18}^-$ 973.1985, found 973.1967.

Cladophorol D (7): pale red amorphous solid; ^{1}H and ^{13}C NMR data, see Table 3; HRMS (ESI) *m/z* $[M − H]^-$ calcd for $C_{60}H_{41}O_{20}^-$ 1081.2197, found 1081.2177.

Cladophorol E (8): pale red amorphous solid; ^{1}H NMR data, see Table 5; ^{13}C NMR data, see Table 4; HRMS (ESI) *m/z* $[M − H]^-$ calcd for $C_{67}H_{43}O_{23}^-$ 1215.2201, found 1215.2188.

Cladophorol F (9): pale red amorphous solid; ^{1}H NMR data, see Table 5; ^{13}C NMR data, see Table 4; HRMS (ESI) *m/z* $[M − H]^-$ calcd for $C_{61}H_{39}O_{21}^-$ 1107.1989, found 1107.1973.

Cladophorol G (10): pale red amorphous solid; ^{1}H NMR data, see Table 5; ^{13}C NMR data, see Table 4; HRMS (ESI) *m/z* $[M − H]^-$ calcd for $C_{73}H_{47}O_{25}^-$ 1323.2412, found 1323.2394.

Cladophorol H (11): pale red amorphous solid; ^{1}H NMR data, see Table 5; ^{13}C NMR data, see Table 4; HRMS (ESI) *m/z* $[M − H]^-$ calcd for $C_{79}H_{51}O_{27}^-$ 1431.2623, found 1431.2617.

Cladophorol I (12): pale red amorphous solid; ^{1}H NMR data, see Table 5; ^{13}C NMR data, see Table 4; HRMS (ESI) *m/z* $[M − H]^-$ calcd for $C_{85}H_{55}O_{29}^-$ 1539.2834, found 1539.2797.

Computational Methods. Model compounds (**1, 13, 14, 15a**, and **15b**) were subjected to a Monte Carlo conformational search using the MMFF94 force field in Spartan '16.[30] The geometry of all conformers within 21 kJ/mol were optimized using density functional theory (DFT) in the Gaussian D09 package,[31] using the B3LYP/6-31G(d) level of theory. Solvent interactions, either DMSO (**1, 13, 14**) or MeOH (**15a, 15b**), were considered with PCM. Frequencies computation was performed to ascertain true minima were obtained (zero imaginary frequency), and the resulting free energies were extracted to calculate the Boltzmann distribution. All conformers representing more than 2% of the population were considered for the computation of the shielding tensors which was performed at the mPW1PW91/6-311+G(d,p) level of theory. The shielding tensors (GIAO) were averaged using their respective Boltzmann weight, and the chemical shifts were finally derived by scaling the shielding tensors against the experimental values.

Pharmacological Assays. Antibacterial and antifungal assays were performed as previously described[32] using methicillin-resistant *Staphylococcus aureus* (MRSA, ATCC 33591), vancomycin-resistant *Enterococcus faecium* (VREF, ATCC 700221), *Escherichia coli* (EC, ATCC 25922), MDR *Escherichia coli* (MDREC, ATCC BAA-1743), wild type *Candida albicans* (WTCA, ATCC 32354), and amphotericin B-resistant *C. albicans* (ARCA, ATCC 90873). The positive controls used were vancomycin for MRSA (MIC < 4 μg/mL), chloramphe-

nicol for VREF (MIC < 8 μg/mL) and EC (MIC < 8 μg/mL), nitrofurantoin for MDREC (MIC = 14 $\pm$ 1 μg/mL), amphotericin B for WTCA (MIC = 16 $\pm$ 1 μg/mL), and nystatin/cycloheximide for ARCA (MIC > 500 μg/mL). Activities were expressed as a 95% confidence interval of concentration required for at least 90% inhibition of growth (MIC$_{90}$).

Additional antibacterial assays were performed using MDR *Klebsiella pneumonia* (MDRKP1, CDC0087), MDR *K. pneumonia* (MDRKP2, CDC0003), MDR *Acinobacter baumannii* (MDRAB1, CDC0280), MDR *A. baumannii* (MDRAB2, CDC0033), MDR *Enterobacter aerogenes* (MDREA, CDC0018), MDR *Enterobacter cloacae* (MDRECL, CDC0050), and wild type *Pseudomonas aeruginosa* (WTPA, PAO1). The bacterial cultures were grown in tryptic soy broth (TSB). Minimum inhibitory concentrations were evaluated with cation-adjusted Mueller Hinton broth (CAMHB) following Clinical and Laboratory Standards Institute (CLSI) methods.[33] Overnight cultures were standardized by optical density (OD) to 5×10^5 CFU/mL, and this was confirmed by plate counts of colonies. MIC values was assigned as described;[34] this was determined by reading at an OD600 nm in a Cytation 3 multimode plate reader after 18−22 h incubation. Gentamicin was used as a positive control.

The human keratinocyte cell line (HaCaT) was maintained, and cytotoxicity of isolated compounds were assessed using LDH cytotoxicity assay as previously described.[34]

Antimalarial activity was assessed using a standard parasite proliferation assay with asexual blood-stage *P. falciparum* and SYBR Green detection.[22] Screening media (complete media supplemented with 0.05% Albumax II but without human serum) and fresh O$^+$ erythrocytes (TSRI Normal Blood Donation) were used for cultures of *P. falciparum* strain Dd2L (gift from Dr. David Fidock, Colombia University). A Labcyte ECHO acoustic liquid handler transferred compounds into assay plates. The plates were inoculated (Multi-Flo; BioTek, VT) with parasitized erythrocytes and fresh erythrocytes prepared in screening media, resulting in a final parasitemia of 0.3% and hematocrit of 2.5%. A chamber with a low oxygen gas mixture at 37 °C was used to culture the assay plates for 72 h with daily gas exchanges. SYBR Green lysis buffer was added to the wells after incubation using a Multi-Flo liquid dispenser, and plates were incubated at room temperature for an additional 24 h to achieve optimal development of the fluorescence signal which was read by an Envision Multimode Reader (PerkinElmer, MA). The positive controls used were atovaquone (EC$_{50}$ = 0.0006 μM) and artemisinin (EC$_{50}$ = 0.03 μM).

ASSOCIATED CONTENT

Ⓢ Supporting Information

The Supporting Information is available free of charge on the ACS Publications website at DOI: 10.1021/acs.joc.8b03218.

> Phylogenetic relationship of G-1240 with other species of the genus *Cladophora*; key HMBC correlations for compounds 5, 6, 8, and 10; dose−response curves of 3−12 against multiple cell lines; spectroscopic data (NMR, MS, UV) for compounds 3−12; DFT energies and geometries for compounds 1, 13, 14, 15a, and 15b; NMR spectroscopic data comparison between 6 and 15a/15b (PDF)
>
> NMR FIDs for all isolated compounds (ZIP)

AUTHOR INFORMATION

Corresponding Author

*E-mail: julia.kubanek@biosci.gatech.edu.

ORCID Ⓘ

Serge Lavoie: 0000-0002-7792-9737
Brandon Dale: 0000-0003-0203-2105
Julia Kubanek: 0000-0003-4482-1831

Notes

The authors declare no competing financial interest.

DEDICATION

This paper is dedicated to William Aalbersberg, in memoriam, for his active mentoring of junior scientists, for his engaged international collaborations, and for his advocacy on behalf of Fijian science and society.

REFERENCES

(1) Quideau, S.; Deffieux, D.; Douat-Casassus, C.; Pouységu, L. Plant Polyphenols: Chemical Properties, Biological Activities, and Synthesis. *Angew. Chem., Int. Ed.* **2011**, *50*, 586−621.

(2) Hertweck, C. The Biosynthetic Logic of Polyketide Diversity. *Angew. Chem., Int. Ed.* **2009**, *48*, 4688−4716.

(3) Ferreira, D.; Slade, D. Oligomeric Proanthocyanidins: Naturally Occurring *O*-Heterocycles. *Nat. Prod. Rep.* **2002**, *19*, 517−541.

(4) Haslam, E.; Cai, Y. Plant Polyphenols (Vegetable Tannins): Gallic Acid Metabolism. *Nat. Prod. Rep.* **1994**, *11*, 41−66.

(5) Arnold, T. M.; Targett, N. M. Marine Tannins: The Importance of a Mechanistic Framework for Predicting Ecological Roles. *J. Chem. Ecol.* **2002**, *28*, 1919−1934.

(6) Boerjan, W.; Ralph, J.; Baucher, M. Lignin Biosynthesis. *Annu. Rev. Plant Biol.* **2003**, *54*, 519−546.

(7) Weng, J. K.; Chapple, C. The Origin and Evolution of Lignin Biosynthesis. *New Phytol.* **2010**, *187*, 273−285.

(8) Martone, P. T.; Estevez, J. M.; Lu, F.; Ruel, K.; Denny, M. W.; Somerville, C.; Ralph, J. Discovery of Lignin in Seaweed Reveals Convergent Evolution of Cell-Wall Architecture. *Curr. Biol.* **2009**, *19*, 169−175.

(9) Blunt, J. W.; Carroll, A. R.; Copp, B. R.; Davis, R. A.; Keyzers, R. A.; Prinsep, M. R. Marine Natural Products. *Nat. Prod. Rep.* **2018**, *35*, 8−53.

(10) Lavoie, S.; Brumley, D.; Alexander, T. S.; Jasmin, C.; Carranza, F. A.; Nelson, K.; Quave, C. L.; Kubanek, J. Iodinated Meroditerpenes from a Red Alga *Callophycus* sp. *J. Org. Chem.* **2017**, *82*, 4160−4169.

(11) Amsler, C. D.; Fairhead, V. A. Defensive and Sensory Chemical Ecology of Brown Algae. *Adv. Bot. Res.* **2005**, *43*, 1−91.

(12) Gómez, I.; Huovinen, P. Induction of Phlorotannins During UV Exposure Mitigates Inhibition of Photosynthesis and DNA Damage in the Kelp *Lessonia nigrescens*. *Photochem. Photobiol.* **2010**, *86*, 1056−1063.

(13) Chen, J. L.; Gerwick, W. H.; Schatzman, R.; Laney, M. Isorawsonol and Related IMP Dehydrogenase Inhibitors from the Tropical Green Alga Avrainvillea Rawsonii. *J. Nat. Prod.* **1994**, *57*, 947−952.

(14) Carte, B. K.; Troupe, N.; Chan, J. A.; Westley, J. W.; Faulkner, D. J. Rawsonol, an Inhibitor of HMG-CoA Reductase from the Tropical Green Alga *Avrainvillea rawsoni. Phytochemistry* **1989**, *28*, 2917−2919.

(15) Sun, H. H.; Paul, V. J.; Fenical, W. Avrainvilleol, a Brominated Diphenylmethane Derivative with Feeding Deterrent Properties from the Tropical Green Alga *Avrainvillea longicaulis. Phytochemistry* **1983**, *22*, 743−745.

(16) Feng, Y.; Carroll, A. R.; Addepalli, R.; Fechner, G. A.; Avery, V. M.; Quinn, R. J. Vanillic Acid Derivatives from the Green Algae *Cladophora socialis* as Potent Protein Tyrosine Phosphatase 1B Inhibitors. *J. Nat. Prod.* **2007**, *70*, 1790−1792.

(17) Charisiadis, P.; Primikyri, A.; Exarchou, V.; Tzakos, A.; Gerothanassis, I. P. Unprecedented Ultra-High-Resolution Hydroxy Group ^{1}H NMR Spectroscopic Analysis of Plant Extracts. *J. Nat. Prod.* **2011**, *74*, 2462−2466.

(18) Weidner-Wells, M. A.; Altom, J.; Fernandez, J.; Fraga-Spano, S. A.; Hilliard, J.; Ohemeng, K.; Barrett, J. F. DNA Gyrase Inhibitory Activity of Ellagic Acid Derivatives. *Bioorg. Med. Chem. Lett.* **1998**, *8*, 97−100.

(19) Lodewyk, M. W.; Siebert, M. R.; Tantillo, D. J. Computational Prediction of ^{1}H and [13]C Chemical Shifts: A Useful Tool for Natural Product, Mechanistic, and Synthetic Organic Chemistry. *Chem. Rev.* **2012**, *112*, 1839−1862.

(20) Reddy, D. S.; Kutateladze, A. G. Structure Revision of an Acorane Sesquiterpene Cordycepol A. *Org. Lett.* **2016**, *18*, 4860−4863.

(21) Grimblat, N.; Zanardi, M. M.; Sarotti, A. M. Beyond DP4: An Improved Probability for the Stereochemical Assignment of Isomeric Compounds Using Quantum Chemical Calculations of NMR Shifts. *J. Org. Chem.* **2015**, *80*, 12526−12534.

(22) Plouffe, D.; Brinker, A.; McNamara, C.; Henson, K.; Kato, N.; Kuhen, K.; Nagle, A.; Adrián, F.; Matzen, J. T.; Anderson, P.; Nam, T. G.; Gray, N. S.; Chatterjee, A.; Janes, J.; Yan, S. F.; Trager, R.; Caldwell, J. S.; Schultz, P. G.; Zhou, Y.; Winzeler, E. A. In silico activity profiling reveals the mechanism of action of antimalarials discovered in a high-throughput screen. *Proc. Natl. Acad. Sci. U. S. A.* **2008**, *105*, 9059−9064.

(23) Bharti, S. K.; Roy, R. Quantitative ^{1}H NMR Spectroscopy. *TrAC, Trends Anal. Chem.* **2012**, *35*, 5−26.

(24) Littler, D. S.; Littler, M. M. *South Pacific Reef Plants: A Divers' Guide to the Plant Life of South Pacific Coral Reefs*; OffShore Graphic, Inc.: Washington, D.C., 2003.

(25) White, T. J.; Bruns, T.; Lee, S.; Taylor, J. Amplification and Direct Sequencing of Fungal Ribosomal RNA Genes for Phylogenetics. In *PCR protocols − A guide to methods and applications*; Innis, M. A., Gelfand, D. H., Sninsky, J. J., White, T. J., Eds.; Academic Press: New York, 1990; p 315−322.

(26) Huang, X.; Madan, A. CAP3: A DNA Sequence Assembly Program. *Genome Res.* **1999**, *9*, 868−877.

(27) Altschul, S. F.; Gish, W.; Miller, W.; Myers, E. W.; Lipman, D. J. Basic Local Alignment Search Tool. *J. Mol. Biol.* **1990**, *215*, 403−410.

(28) Kumar, S.; Stecher, G.; Li, M.; Knyaz, C.; Tamura, K. MEGA X: Molecular Evolutionary Genetics Analysis Across Computing Platforms. *Mol. Biol. Evol.* **2018**, *35*, 1547−1549.

(29) Tamura, K.; Nei, M. Estimation of the Number of Nucleotide Substitutions in the Control Region of Mitochondrial DNA in Humans and Chimpanzees. *Mol. Biol. Evol.* **1993**, *10*, 512−526.

(30) *Spartan'16*; Wavefunction, Inc.: Irvine, CA.

(31) Frisch, M. J.; Trucks, G. W.; Schlegel, H. B.; Scuseria, G. E.; Robb, M. A.; Cheeseman, J. R.; Scalmani, G.; Barone, V.; Mennucci, B.; Petersson, G. A.; Nakatsuji, H.; Caricato, M.; Li, X.; Hratchian, H. P.; Izmaylov, A. F.; Bloino, J.; Zheng, G.; Sonnenberg, J. L.; Hada, M.; Ehara, M.; Toyota, K.; Fukuda, R.; Hasegawa, J.; Ishida, M.; Nakajima, T.; Honda, Y.; Kitao, O.; Nakai, H.; Vreven, T.; Montgomery, J. A., Jr.; Peralta, J. E.; Ogliaro, F.; Bearpark, M.; Heyd, J. J.; Brothers, E.; Kudin, K. N.; Staroverov, V. N.; Keith, T.; Kobayashi, R.; Normand, J.; Raghavachari, K.; Rendell, A.; Burant, J. C.; Iyengar, S. S.; Tomasi, J.; Cossi, M.; Rega, N.; Millam, J. M.; Klene, M.; Knox, J. E.; Cross, J. B.; Bakken, V.; Adamo, C.; Jaramillo, J.; Gomperts, R.; Stratmann, R. E.; Yazyev, O.; Austin, A. J.; Cammi, R.; Pomelli, C.; Ochterski, J. W.; Martin, R. L.; Morokuma, K.; Zakrzewski, V. G.; Voth, G. A.; Salvador, P.; Dannenberg, J. J.; Dapprich, S.; Daniels, A. D.; Farkas, O.; Foresman, J. B.; Ortiz, J. V.; Cioslowski, J.; Fox, D. J. *Gaussian 09*, Revision D.01; Gaussian: Wallingford CT, 2009.

(32) Kubanek, J.; Prusak, A. C.; Snell, T. W.; Giese, R. A.; Hardcastle, K. I.; Fairchild, C. R.; Aalbersberg, W.; Raventos-Suarez, C.; Hay, M. E. Antineoplastic Diterpene-Benzoate Macrolides from the Fijian Red Alga *Callophycus serratus. Org. Lett.* **2005**, *7*, 5261−5264.

(33) CLSI. *Performance Standards for Antimicrobial Susceptibility Testing*; 23rd Informational Supplement. CLSI document M100-S25; Clinical and Laboratory Standards Institute: Wayne, PA, 2013.

(34) Quave, C. L.; Lyles, J. T.; Kavanaugh, J. S.; Nelson, K.; Parlet, C. P.; Crosby, H. A.; Heilmann, K. P.; Horswill, A. R. *Castanea sativa* (European Chestnut) Leaf Extracts Rich in Ursene and Oleanene Derivatives Block *Staphylococcus* aureus Virulence and Pathogenesis without Detectable Resistance. *PLoS One* **2015**, *10*, e0136486.

■ NOTE ADDED AFTER ASAP PUBLICATION

A Supporting Information file containing NMR FIDs was added on April 9, 2019.